https://doi.org/10.5194/egusphere-2024-831
Preprint. Discussion started: 13 May 2024
© Author(s) 2024. CC BY 4.0 License.

Three-dimensional discrete element simulations on pressure ridge formation

Marek Muchow[1] and Arttu Polojärvi[1]

[1]Aalto University, School of Engineering, Department of Mechanical Engineering, P.O. Box 14100, FI-00076 Aalto, Finland

Correspondence: Marek Muchow (marek.muchow@aalto.fi)

Abstract. This study presents the first three-dimensional discrete element method simulations on pressure ridge formation. Pressure ridges are an important feature of the sea-ice cover, as they contribute to the mechanical thickening of ice and likely limit the strength of sea ice in large scale. We validate the simulations against laboratory-scale experiments, confirming their accuracy in predicting ridging forces and ridge geometries. Then we demonstrate that Cauchy-Froude scaling applies for translating laboratory-scale results on ridging to full-scale scenarios. We show that non-simultaneous failure, where an ice sheet fails at distinct locations across the ridge length, is required for an accurate representation of the ridging process. This process cannot be described by two-dimensional simulations. We also find a linear relationship between the ridging forces and the ice thickness, contrasting with earlier results in the literature obtained by two-dimensional simulations.

1 Introduction

In this study, we simulate pressure ridge formation by using a three-dimensional discrete element method (DEM) (Cundall and Strack, 1979) model for the first time. Pressure ridging is an ice failure process resulting from relative compression of two or more ice floes driven by winds and currents. Ridges may also form as a result of failure of an intact ice sheet. Thus, ridges consist of ice rubble formed by ice fragments accumulated in a keel underwater, and a sail on top of the ice (Figure 1). Ridging is assumed to be one of the main mechanisms limiting large-scale strength of sea ice (Lipscomb et al., 2007), it influences the local ice thickness (Leppäranta and Hakala, 1992), and it increases the overall sea-ice volume (Itkin et al., 2018; von Albedyll et al., 2022). Therefore, ridging has a major role in sea-ice redistribution in Earth System Models (Thorndike et al., 1975; Lipscomb et al., 2007). Understanding ridging processes is, thus, of utmost importance for sea-ice dynamics. Additionally, understanding ridging processes is important to resolve ridges accurately in high-resolution forecasting simulations as needed, for example, for planning ship routes and locations for offshore wind farms.

First theoretical models for ridging were established in the 1970s with the kinematic ridging model by Parmerter and Coon (1972). More recent developments focus on the representation of ridging in Earth System models (Roberts et al., 2019). While

https://doi.org/10.5194/egusphere-2024-831
Preprint. Discussion started: 13 May 2024
© Author(s) 2024. CC BY 4.0 License.

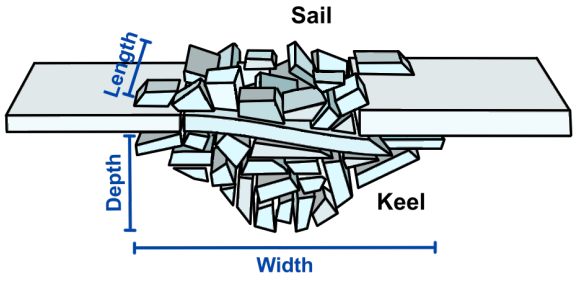

Figure 1. Sketch of a pressure ridge and its main dimensions depth, width and length.

these models are based on mathematical relationships between different processes involved in ridging, DEM models offer insight into the process itself.

Earlier simulation-based studies on ridging have used two-dimensional DEM models. Hopkins et al. (1991) simulated ridging by compression of ice rubble between two floes. In further simulations by Hopkins (1994, 1998), a thin, intact, lead ice was pushed against a thick ice floe and went through a continuous ice failure process to form a ridge. Hopkins et al. (1999) simulated the formation of a ridge due to compression of ice sheets of similar, but nonuniform, ice thickness. Importantly, these simulations suggested a relation $F \propto h^{3/2}$ between the ridging force, F, and ice thickness, h, which has been used since in some Earth System Models to define the strength of ice of a given thickness (Lipscomb et al., 2007).

Our study is the first to utilize three-dimensional DEM simulations to investigate ridging (Figure 2). In two-dimensional simulations, one cross-section of a ridge across its width is usually modelled, while three-dimensional studies can take the length of a ridge into account (Figure 1). First, we successfully validated our simulations by comparing our results to those obtained experimentally by Tuhkuri and Lensu (2002). To study full-scale ridging, we performed simulations using the same material parameters and ice thicknesses from laboratory scale upscaled to full scale, that is, to the scale of natural ice ridges. This upscaling is based on Cauchy-Froude scaling, typically used in studies on ice-structure interaction (Schwarz, 1977; Timco, 1984). We show with these simulations that Cauchy-Froude scaling applies also for ridging. This finding gives confidence to our full-scale simulation results, opens an important avenue for future experimental work, and sheds light on complex mechanics related to ridging processes. Further, we show that three-dimensional simulations indicate a relation $F \propto h$ between ridging force and ice thickness.

In what follows, we first briefly describe the model and introduce the setup for the simulations in laboratory- and full-scale in Section 2. Next, we present the results of the validation study and full-scale simulations in Section 3. We then discuss the results in Section 4 before concluding in Section 5.

https://doi.org/10.5194/egusphere-2024-831
Preprint. Discussion started: 13 May 2024
© Author(s) 2024. CC BY 4.0 License.

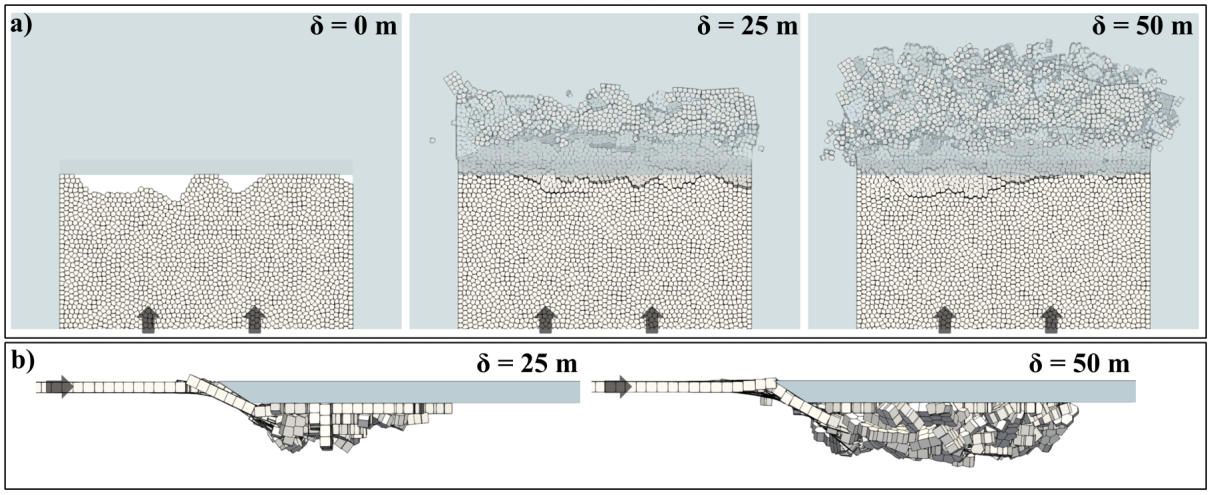

Figure 2. Snapshots from a DEM simulation of full-scale ridging viewed from the top (a) and side (b) at different stages of ice pushed δ into the ridge. Here 0.95 m thick ice (light gray) fails against a rigid ice floe (light blue). The ice moves in the direction of the rigid ice floe as indicated by the arrows. The simulation setup is described in detail in Section 2.2.

2 Methods

This section first describes our three-dimensional DEM model briefly. Then it explains the setups for ridging simulations in laboratory and full scale.

2.1 Numerical model

The numerical model employed is a three-dimensional discrete element method (DEM) code described in detail by Polojärvi (2022). The model was verified to describe the response and the fracture of an ice floe by Lilja et al. (2019a, b, 2021) and its results were successfully validated against laboratory-scale ice-structure interaction experiments by Polojärvi (2022). On a general level, the model implementation is rather standard for DEM, as a central difference scheme is utilized for explicit time-stepping, rigid discrete particles interact through pairwise contacts, and deformation is described by using deformable finite elements connecting the rigid particles. The forces applied on the particles include internal forces due to ice deformation, contact forces and external forces due to gravity, buoyancy, and water drag.

In more detail, the deformable ice floe was simulated by employing a lattice of rigid, discrete particles interconnected by three-dimensional Timoshenko beam elements. The particles used are convex polyhedrons, generated through centroidal Voronoi tesselation (Du et al., 1999). The beam elements connect pairs of particles sharing a face. Both translational and rotational degrees of freedom of the beams correspond to those of the connected particles. The implementation of the beams follows Crisfield (1990, 1997). Ice deformation and failure stem from the individual beams undergoing deformation and failure due to relative motion of the pair of particles connected by each beam. In the elastic regime, viscous material damping is used.

https://doi.org/10.5194/egusphere-2024-831
Preprint. Discussion started: 13 May 2024
© Author(s) 2024. CC BY 4.0 License.

Once the stress state of a beam meets a prescribed mixed-mode failure criterion (Schreyer et al., 2006), the beam undergoes a cohesive softening process, resulting in energy dissipation upon fracture (Paavilainen et al., 2009).

The model employs a soft-contact approach, wherein the contact force between a pair of interacting particles is determined based on a small particle-particle overlap volume, with the point of application of the force located at the centroid of this overlap volume. The contact force, $\mathbf{f} = \mathbf{f}_n + \mathbf{f}_t$, has a normal and a tangential component, $\mathbf{f}_n$ and $\mathbf{f}_t$, respectively. $\mathbf{f}_n$ is solved using an elastic-viscous-plastic contact force model by Hopkins (1992). The elastic and viscous portions of $\mathbf{f}_n$ are, respectively, calculated by using the gradient of overlap volume and its rate of change (Feng et al., 2012; Feng, 2021). The plastic portion of $\mathbf{f}_n$, describing local yielding at contacts, is solved based on contact area. Tangential compliance and friction between the particles contribute to the tangential force $\mathbf{f}_t$ (Hopkins, 1992). The contact model is parameterized by using the material properties of ice as described in Polojärvi (2022).

2.2 Ridging simulations

This section first describes the setup of the simulations used to model the laboratory-scale experiments conducted by Tuhkuri and Lensu (2002). Then we describe how we upscale the setup and input parameters to full-scale by utilizing Cauchy-Froude scaling and perform simulations in full scale.

2.2.1 Laboratory-scale

We validated our simulations by comparing their ridging force levels and ridge profiles to those yielded by the laboratory-scale experiments by Tuhkuri and Lensu (2002). The experiments were conducted at the Aalto Ice and Wave Tank, an ice basin with an area of $40 \times 40\,\mathrm{m}$. In the experiments, 13 ice sheets were used to perform 38 experiments in total. In the experiments, each sheet was first cut into three $6\,\mathrm{m}$-wide strips with the surrounding ice left in place. The strips were then cut in half and one of the floes was pushed against the other one. The horizontal force required to move the floe was recorded and defined as the ridging force, F, measured as the function of the amount of ice pushed, δ. From these experiments, we chose four sets, S1 ... S4, of three experiments each, which all resulted in ridging. The material parameters, tensile strength, σ_f, and elastic modulus, E, and the ice thickness h varied between these sets (Table 1). The total δ at the end of the experiments varied between $4.2\,\mathrm{m}$ and $12.0\,\mathrm{m}$. The ridges in sets S1 and S2 had their profiles measured at the end of the experiments at three equally spaced locations along the length of the ridge.

The simulation setup featured a deformable ice floe moving at a constant velocity towards a rigid floe (Figure 2), from which we measured the ridging force F. Similar to the experiments, additional ice floes on each side restricted the moving floe from lateral motion. There was a $1\,\mathrm{cm}$ gap between the moving floe and the floes on the sides to avoid frictional resistance. The deformable floe had an uneven edge, while the rigid ice floe had a downward-sloping even edge at an angle of about $30°$ from the horizontal. These features were implemented ad hoc to avoid excessively high peaks in F at the initial contact of the floes and to replicate the soft underside of the laboratory-scale ice. The thickness of the rigid floe was four times that of the deformable floe to avoid extensive rafting. The particles had an average aspect ratio of 1.5 between the ice thickness and

https://doi.org/10.5194/egusphere-2024-831
Preprint. Discussion started: 13 May 2024
© Author(s) 2024. CC BY 4.0 License.

Table 1. Four sets S1 ... S4 of parameterizations chosen after the laboratory-scale experiments by Tuhkuri and Lensu (2002). In the table, h is the ice thickness, and E and σ_f are the elastic modulus, and tensile strength, respectively. Other main parameters are given in Table 2.

set	h [m]	E [MPa]	σ_f [kPa]
S1	0.095	27	10
S2	0.089	24	16
S3	0.078	64	12
S4	0.048	368	37

their width, defining the minimum aspect ratio for an ice block in our simulations. This choice allowed the aspect ratio of the simulated ice to adhere to the observed aspect ratio of 3.5 ± 2.0 for ridges in the Barents Sea (Høyland, 2007).

Similarly to the experiments, we performed four sets of simulations, S1 ... S4. While the parameters, which varied between S1 ... S4, were already given in Table 1, other simulation parameters are presented in Table 2. We repeated the simulations five times for each parameterization. In the repeated simulations, the tessellation and the shape of the edge of the deformable ice sheet were varied, which were enough for the simulations to yield different failure processes as described in Polojärvi (2022). While in the experiments the ice was pushed with velocity of $0.01\,\mathrm{m\,s^{-1}}$, it was also shown that the ice velocity, at least in the range $0.01 \ldots 0.06\,\mathrm{m\,s^{-1}}$ tested, did not affect the results (Tuhkuri and Lensu, 2002). Thus, we used $0.05\,\mathrm{m\,s^{-1}}$ as the ice velocity in our simulations. Finally, the simulated ice floes were of uniform thickness, while Tuhkuri and Lensu (2002) used ice of uneven thickness in their experiments. We accounted for the effect of varying ice thickness on frictional sliding by using an ice-ice friction coefficient of 0.6, which is at the high, but realistic, end for the values measured for ice (Sukhorukov and Løset, 2013).

2.2.2 Full-scale

To discuss the implications of the results below one must know how ridging processes scale; the relevant question to ask is if measured laboratory-scale (LS) ridging forces can be used to estimate those in full-scale (FS). Cauchy-Froude scaling, often used to scale experiments featuring ice-going ships and offshore structures, was also used here for the upscaling and later evaluated. In brief, with Cauchy-Froude scaling, geometric, kinematic and dynamic similitude are preserved (Schwarz, 1977; Timco, 1984). The Froude and Cauchy numbers are, respectively, given by

$$Fr = \frac{v}{\sqrt{gl}} \qquad \text{and} \qquad Ca = \frac{\rho v^2}{E}. \tag{1}$$

Fr describes ratio of inertia to gravitational forces, represented, respectively, by velocity v and gravitational acceleration g and length scale l. Ca, on the other hand, describes the ratio between inertia, represented by the density ρ and velocity v, and elastic forces, represented by the elastic modulus E.

https://doi.org/10.5194/egusphere-2024-831
Preprint. Discussion started: 13 May 2024
© Author(s) 2024. CC BY 4.0 License.

Table 2. Main simulation parameters in the laboratory-scale simulations. Parameters are described in detail in Polojärvi (2022).

Description		Value	Unit
General	Time step	$2 \cdot 10^{-5}$	s
	Gravitational acceleration	9.81	$\mathrm{m\,s^{-2}}$
Ice	Sheet width	6	m
	Sheet length	18 ... 25	m
	Density	930	$\mathrm{kg\,m^{-3}}$
	Velocity	0.05	$\mathrm{m\,s^{-1}}$
Beams	Damping ratio	0.75	
	Shear strength	σ_f	
	Poisson's ratio	0.3	
	Mean length	$1.5h$	m
Contact	Plastic limit	40	kPa
	Ice-ice friction	0.6	
Water	Density	1000	$\mathrm{kg\,m^{-3}}$
	Drag coefficient	1.0	

To test if Cauchy-Froude scaling is applicable, we first upscaled the parameters from LS to FS. Thus, all LS parameters (Table 1), including the ice thickness, material parameters and velocity, were upscaled using the scaling parameter λ:

$$h_{FS} = \lambda h_{LS}, \quad \sigma_{FS} = \lambda \sigma_{LS}, \quad E_{FS} = \lambda E_{LS}, \quad \text{and} \quad v_{FS} = \lambda^{1/2} v_{LS}. \tag{2}$$

The ice-ice friction was kept constant. If Cauchy-Froude scaling applies for ridging processes, then FS simulations should yield ridging forces matching those from LS simulations through scaling

$$F_{FS} = \lambda^3 F_{LS}. \tag{3}$$

For the FS simulations here, we used $\lambda = 10$ based on Tuhkuri and Lensu (2002). We did not directly scale mean particle size, but instead used a mean aspect ratio of one for the particles in FS simulations, since preliminary simulations showed occasional sharp force peaks with large particles. The peaks were likely due to the limited capability of the model to simulate local crushing and fragmentation of large particles (Polojärvi, 2022; Prasanna and Polojärvi, 2023). Through additional simulations we saw that the average ridging force was not affected by this choice. Further, the thickness of the rigid floe was adjusted to a maximum of $2\,\mathrm{m}$. The thickness of the rigid floe was found to not influence the magnitude of the mean ridging force.

3 Results

We first show that the results from our simulations compare well with laboratory-scale experiments in regards to ridging forces and ridge geometries. Next, we use the simulations to show that Cauchy-Froude scaling applies to ice ridging.

https://doi.org/10.5194/egusphere-2024-831
Preprint. Discussion started: 13 May 2024
© Author(s) 2024. CC BY 4.0 License.

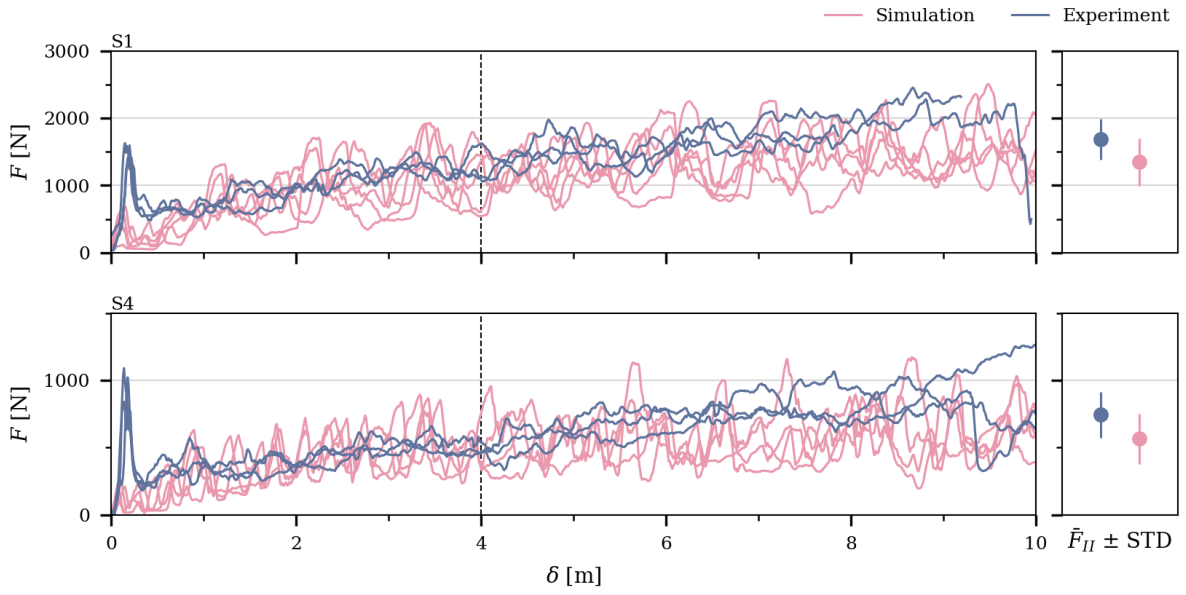

Figure 3. Ridging force, F, as a function of the amount of ice pushed, δ, from the simulations and experiments with the thickest and thinnest ice (parameter sets S1 and S4, respectively). Each graph shows $F - \delta$ record from five laboratory-scale simulations and three experiments. The vertical line illustrates the approximate δ where the phase of the process changed from the initial phase to the second phase with the mean force $\bar{F}_{II} \pm$ one standard deviation (STD) for the second phase given in the right column.

3.1 Laboratory-scale

Figure 3 shows ridging force, F, plotted against the length of ice pushed, δ, in the simulations and the experiments. Only the $F - \delta$ records from the simulations and the experiments with the thickest ice and thinnest ice are shown, but these are representative for all data. Excluding the initial peak in the experimental $F - \delta$ records, the ridging-force levels from the experiments and simulations are in good agreement, which already suggests that our simulations describes ridging well and thus partly validates our approach. The initial peak in experimental $F - \delta$ records is due to the two ice floes with even edges colliding and it is not expected to be present in data from the simulations (Section 2.2.1). It should be emphasized that the initial peak F should not be treated as a ridging force, since it does not represent the force required to build a ridge.

The $F - \delta$ records could be divided into an initial phase, during which F increased with δ, followed by a second phase of F fluctuating about a constant mean. During the initial phase, F increased with an approximately equal rate in the simulations and the experiments. The first phase continued up to $\delta \approx 4$ m and terminated at the dashed line in $F - \delta$ records of Figure 3. The change from the initial to second phase is more distinct in the simulations than in the experiments. During the second phase, F can be seen to fluctuate around a mean force, $\bar{F}_{II}$. Magnitude of $\bar{F}_{II}$ in the simulations and the experiments compares well (Figure 3): $\bar{F}_{II}$ from the simulations is within one standard deviation of that in the experiments.

https://doi.org/10.5194/egusphere-2024-831
Preprint. Discussion started: 13 May 2024
© Author(s) 2024. CC BY 4.0 License.

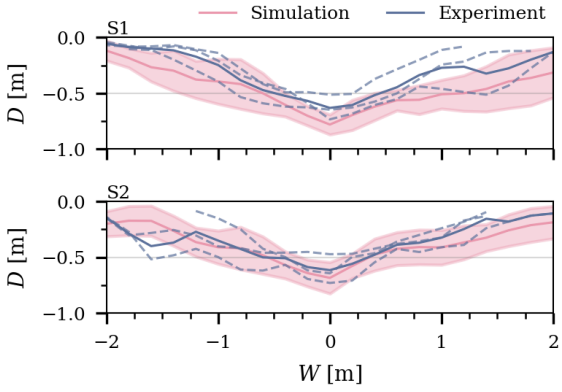

Figure 4. Comparison of mean ridge profiles (solid lines) from the experiments and simulations. All three ridge profiles per ridge for the experiments are displayed with dashed lines, while the standard deviation calculated from five simulated profiles is displayed as shading.

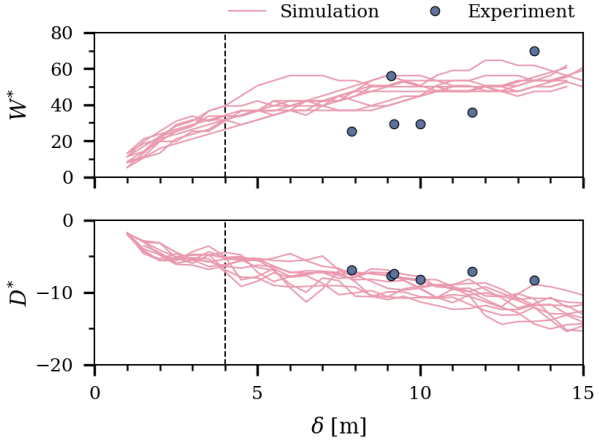

Figure 5. Evolution of the normalized ridge width $W^* = W/h$ and depth $D^* = D/h$ from S1 and S2 laboratory-scale simulations. Data are normalized by ice thickness h and plotted against the amount of ice pushed δ. Experimental data were only available for the experiments with parameter sets S1 and S2. Vertical dashed line represents the change from the initial phase to the second phase.

In addition to $F-\delta$ records, Tuhkuri and Lensu (2002) provided results from ridge profile measurements, which we compare to ridge profiles from the simulations in Figure 4. The profiles were available for ridges in sets S1 and S2. For profiles yielding from the simulations, the thickness of the rigid floe is subtracted from the entire profile. Overall, the mean ridge profiles from the simulations are in agreement with the profiles from the experiments in shape and depth (Figure 4). Some ridges in the experiments are shallower than the ones from the simulations. This difference is expected, as the ice in the experiments can crush and fragment into very small pieces, leading to potentially more compacted ice rubble than in the simulations, where the

https://doi.org/10.5194/egusphere-2024-831
Preprint. Discussion started: 13 May 2024
© Author(s) 2024. CC BY 4.0 License.

smallest ice fragment size is governed by the particle size. Nevertheless, the majority of the ridges from the simulations have their profiles within one standard deviation from profiles measured in the experiments.

Additionally, we analyzed how depth and width, D and W, respectively, of the ridge developed as function of δ. D was defined based on the deepest point of the keel with the thickness of the rigid floe subtracted from it. W was defined based on the depth of rubble with $D > 2h$. Figure 5 illustrates how D and W developed for the S1 and S2 sets by showing their thickness-normalized values $W^* = W/h$ and $D^* = D/h$, which accounts for the various values of h used in the simulations. It can be seen that D^* increases throughout the simulated process, while W^* first increases and then plateaus. The moment at which W^* stabilizes coincided with the change in the phase of $F - \delta$ records (Figures 3). Figure 5 also shows experimental data points (S1 and S2) based on the profile measurements at the end of the experiments. Data from the simulations and the experiments can be seen to be in fair agreement.

In addition to the comparison of ridging forces and geometry, the simulations allow observing ridging processes in detail. Each ridging simulation started with the deformable floe approaching the rigid floe, followed by pieces of the uneven edge breaking off. After the initial interaction, the floe started to submerge and break into rubble, which generally accumulated in one layer and could be related to initial rafting. Then, the intact, deformable floe continued to bend downwards and fail, either against the rigid floe or the accumulated ice rubble. After the new ice rubble was created, it moved further under the rigid floe with the ridge growing in depth and width (Figure 5). During this process, the rubble pieces can break and rearrange. Nevertheless, the ice rarely broke into the smallest possible particle size, resulting in rubble pieces consisting of several connected particles. From observations of several ridging simulations, we identified two main deformation processes during ridging: first, creating more ice rubble to be added into the ridge and, second, further deforming and transporting the ice rubble within the ridge.

3.2 Full-scale

Next, we demonstrate that Cauchy-Froude scaling is applicable to ridging. To do this, Figure 6 compares the $F - \delta$ records from FS simulations to those upscaled from LS simulations (Equation 3). This comparison shows that the overall features of the $F - \delta$ records are similar and the force levels in the simulations conducted in different scales are in agreement.

The $F - \delta$ records of Figure 6 again show two phases, with the second phase of $\bar{F}_{II}$ starting at $\delta \approx 40\,\mathrm{m}$. This pattern would be expected if Cauchy-Froude scaling applied for ridging, since the second phase started $\delta \approx 4$ m in LS simulations and scaling factor $\lambda = 10$ was used. As Figure 6 indicates, $\bar{F}_{II}$ from the simulations performed in different scales match well during this phase.

In addition to similar $F - \delta$ records, W and D of FS ridges evolved similarly to LS ridges. Since the main features of ridge geometry were similar in both scales, and the $F - \delta$ records matched with the chosen scaling, we conclude that the model can be applied on both scales and that the Cauchy-Froude scaling applies for ridging process.

https://doi.org/10.5194/egusphere-2024-831
Preprint. Discussion started: 13 May 2024
© Author(s) 2024. CC BY 4.0 License.

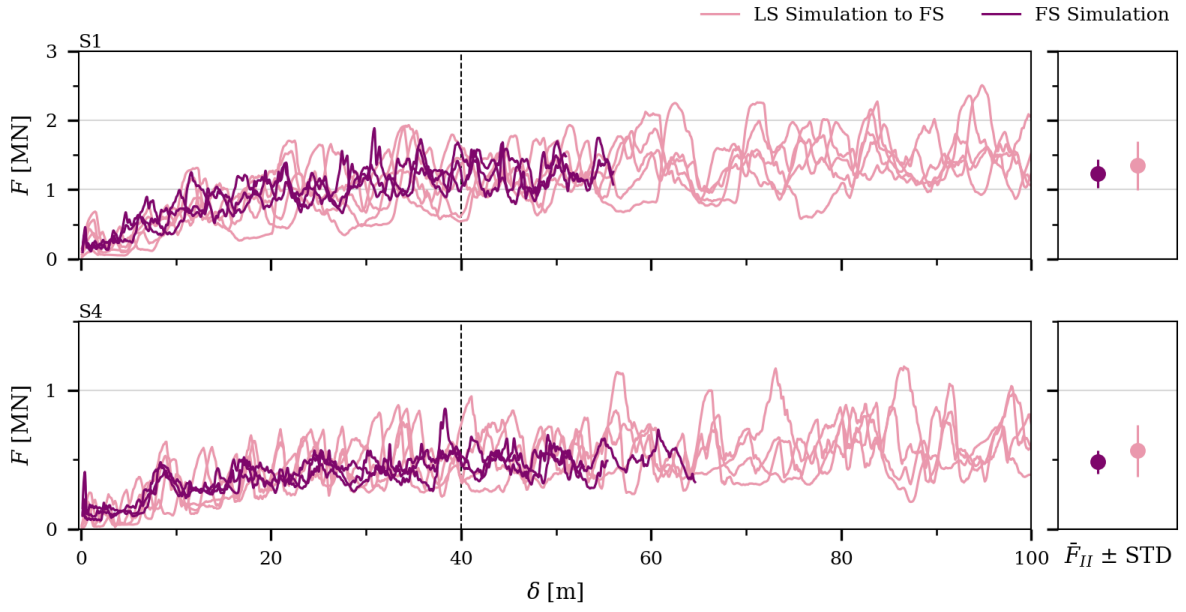

Figure 6. Ridging force, F, as a function of the amount of ice pushed, δ, from laboratory-scale (LS) and full-scale (FS) simulations with the thickest and thinnest ice (parameter sets S1 and S4, respectively). Each graph shows $F-\delta$ record from five LS simulations and three FS simulations. The vertical line illustrates the approximate δ where the phase of the process changed from the initial phase to the second phase with the mean force $\bar{F}_{II}$ ± one standard deviation (STD) for the second phase given in the right column.

4 Discussion

Formation of pressure ridges has been simulated earlier only by utilizing two-dimensional DEM models (Hopkins, 1994, 1998; Hopkins et al., 1999; Damsgaard et al., 2021). Since simulating pressure ridging in three-dimensions is a fairly complex effort, it is relevant to discuss how our results differ from two-dimensional simulations. One important feature only a three-dimensional simulation allows is the non-simultaneous failure process. Non-simultaneous failure is a well-known feature related to sea ice interacting with offshore structures (Ashby and Hallam, 1986; Sanderson, 1988). In this case, the ice floe acting on the structure does not fail uniformly across the whole length of its nominal contact area, defined as hL, but only at distinct locations at any given time instant. In keeping with this analogy, the ice failure in our full-scale simulations never occurred across the whole length of the ridge at once, but rather through seemingly independent smaller failure processes and failure events at distinct locations across the length of the ridge (Figure 2).

A non-simultaneous failure process cannot be described by two-dimensional simulations. Absence of this feature manifests, for example, as abrupt drops in the $F-\delta$ records to zero. These force drops occur when the contact between the interacting ice floes is momentarily lost upon ice failure as seen from results by Hopkins (1998). Our $F-\delta$ records do not show such force drops, but we ran supplementary simulations with shorter ridges. These simulations confirmed that with the decreasing L, the

https://doi.org/10.5194/egusphere-2024-831
Preprint. Discussion started: 13 May 2024
© Author(s) 2024. CC BY 4.0 License.

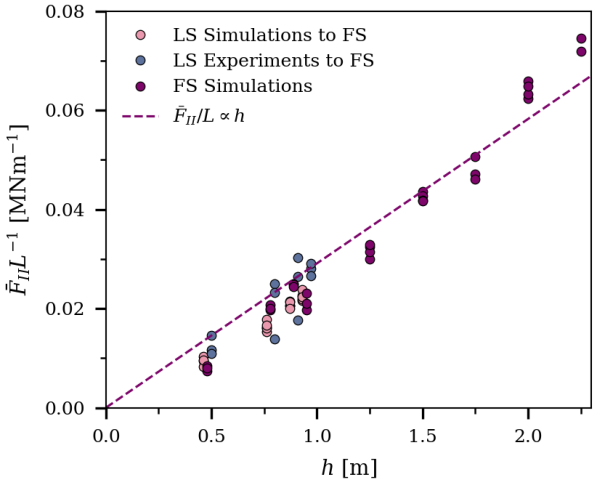

Figure 7. Mean ridging force, $\bar{F}_{II}$, during the second phase ($\delta = 4...10\,\mathrm{m}$) divided by the ridge length L for each individual FS simulation is shown depending on the ice thickness h of the deformable ice. Simulations with $h > 1.0$ m are additional simulations conducted with thicker ice with S1 and S4 material properties (Table 1). The dashed line shows a linear fit applied to the FS data.

fluctuations in the $F - \delta$ records became more pronounced. Simulations with $h = 0.95\,\mathrm{m}$ and $L = 10\,\mathrm{m}$ yielded $F - \delta$ records with about 90 % higher standard deviation for F together with periods of virtually zero F. Non-simultaneous failure, allowed by three-dimensional simulations, is required for realistic modeling of ridge formation and estimates of ridging forces.

Tuhkuri and Lensu (2002) observed that in their experiments ridging started with rafting. Based on this finding, they suggested a simplified ridging model including two phases, the first phase with an increasing F due to rafting and the second phase with a constant F. This concept is supported by dissection of full-scale ridges, which featured several layers of rafted ice close to the waterline as a consolidated layer (Høyland, 2007). This observation made them suggest that rafting is also part of full-scale ridging. Our initial simulations in laboratory-scale showed that our model is prone to yield very extensive rafting, leading us to use the setup as described above. The simulations performed here do not show an initial phase of pure rafting as the ice fails into discrete ice blocks while being submerged. Nevertheless, the later ridge formation process is still described well and the $F - \delta$ records from the simulations match well with those from the experiments. Further, when accounting for the fact that we set up our simulations so that the initial peak force in $F - \delta$ records was removed, it appears that the ridging process and magnitude of $\bar{F}_{II}$ are apparently not affected by the details of the initial stages of pressure ridge formation.

What do our simulations then tell about the mechanisms that limit the magnitude of F? This is an important question related to estimating the large-scale ice strength, which is assumed to be limited by the ice failure processes such as pressure ridge formation (Tuhkuri and Lensu, 2002; Lipscomb et al., 2007). Figure 7 aims to answer this question by plotting the values of average ridging force per unit length, $\bar{F}_{II}L^{-1}$, against h for all simulations and experiments. (Values for $\bar{F}_{II}L^{1}$ from LS simulations presented were scaled to FS according to Equation 3.) Figure 7 shows $\bar{F}_{II}L^{-1}$ for additional FS simulations

https://doi.org/10.5194/egusphere-2024-831
Preprint. Discussion started: 13 May 2024
© Author(s) 2024. CC BY 4.0 License.

with $h > 1.0\,\mathrm{m}$, ran with FS parameterizations of S1 an S4 and preserved L/h ratio of S1 (Table 1). In addition to the data points, Figure 7 presents a linear fit for the full-scale data clearly suggesting $\bar{F}_{II} \propto h$. The linear fit has a Pearson correlation coefficient of 0.99. This result differs from $F \propto h^{3/2}$ found earlier when using two-dimensional DEM simulations (Hopkins, 1998; Damsgaard et al., 2021). Analogue to the inclusion of L into ridging simulations, two- and three-dimensional DEM simulations on ice-structure interaction processes appear to yield a similar behavior. Two-dimensional simulations on ice loading on an inclined structure suggested that the ice load is proportional to $h^{3/2}$, while three-dimensional simulations of ice acting on a cone yield a linear relationship between ice load and h (Ranta et al., 2018; Polojärvi, 2022). Combining these observations, it appears even more crucial to simulate ridging in three dimensions.

From the aspect of improving large-scale compressive ice strength estimates, our results have the following interesting implication. During full-scale simulations, it appears that a L/h ratio of 30, here nearly 1-meter-thick-ice forming a 30-meter-long-ridge, is enough to account for the effect of non-simultaneous failure. This ratio suggests that experimental work for large-scale ridging could be performed in a full-scale setting to further confirm the results presented here and yielded by earlier laboratory-scale work. It is, however, beyond the scope of this paper to start numerically deriving the exact combinations of parameters applicable for executing such experiments.

5 Conclusions

This is the first study to use a three-dimensional discrete element method (DEM) to study pressure ridging. The model used was that originally presented in Polojärvi (2022). Simulations were first ran by using laboratory-scale parametrization, which were then upscaled to full scale by using Cauchy-Froude scaling. Based on the simulation results, we conclude:

- The numerical model was successfully validated by comparing the ridging force records and ridge geometries to laboratory-scale experimental data (Figure 3 and 4).
- Cauchy-Froude scaling is applicable to ridging. This result opens new avenues for experimental studies and gives new insight on mechanics of ridging processes (Figure 6).
- Three-dimensional simulations also account for the ridge length, which facilitates non-simultaneous failure. This expansion is important as it allows modeling realistic ridging processes (Section 4).
- There is a linear relationship, $F \propto h$, between the ridging force and ice thickness. It seems that this finding can only be reached with three-dimensional simulations (Figure 7).

The next steps for our numerical studies on ridging is to enlarge the sea-ice area so that several ridges may form. These simulations would yield crucial information for the large-scale ice strength as used in common Earth System Models.

Author contributions. MM set up the simulations, performed them, analyzed the results, and wrote the paper. AP implemented the DEM code, and contributed to the analysis and writing of the paper.

https://doi.org/10.5194/egusphere-2024-831
Preprint. Discussion started: 13 May 2024
© Author(s) 2024. CC BY 4.0 License.

Competing interests. The authors do not have competing interests.

Acknowledgements. The authors wish to acknowledge funding from the European Union – NextGenerationEU instrument through Academy of Finland under grant number (348586) WindySea – Modelling engine to design, assess environmental impacts, and operate wind farms for ice-covered waters. MM acknowledges funding from the AaltoENG 4-year doctoral program. Additionally, we thank Jukka Tuhkuri and Mikko Lensu for providing us with the experimental data.

https://doi.org/10.5194/egusphere-2024-831
Preprint. Discussion started: 13 May 2024
© Author(s) 2024. CC BY 4.0 License.

References

Ashby, M. F. and Hallam, S. D.: The Failure of Brittle Solids Containing Small Cracks under Compressive Stress States, Acta Metallurgica, 34, 497–510, https://doi.org/10.1016/0001-6160(86)90086-6, 1986.

Crisfield, M. A.: A Consistent Co-Rotational Formulation for Non-Linear, Three-Dimensional, Beam-Elements, Computer Methods in Applied Mechanics and Engineering, 81, 131–150, https://doi.org/10.1016/0045-7825(90)90106-V, 1990.

Crisfield, M. A.: Non-Linear Finite Element Analysis of Solids and Structures: Volume 2: Advanced Topics, Proceedings of the Institution of Mechanical Engineers: Journal of Mechanical Engineering Science, Part C, 211, 489, 1997.

Cundall, P. A. and Strack, O. D. L.: A Discrete Numerical Model for Granular Assemblies, Géotechnique, 29, 47–65, https://doi.org/10.1680/geot.1979.29.1.47, 1979.

Damsgaard, A., Sergienko, O., and Adcroft, A.: The Effects of Ice Floe-Floe Interactions on Pressure Ridging in Sea Ice, Journal of Advances in Modeling Earth Systems, 13, https://doi.org/10.1029/2020ms002336, 2021.

Du, Q., Faber, V., and Gunzburger, M.: Centroidal Voronoi Tessellations: Applications and Algorithms, SIAM Review, 41, 637–676, https://doi.org/10.1137/S0036144599352836, 1999.

Feng, Y. T.: An Energy-Conserving Contact Theory for Discrete Element Modelling of Arbitrarily Shaped Particles: Contact Volume Based Model and Computational Issues, Computer Methods in Applied Mechanics and Engineering, 373, 113 493, https://doi.org/10.1016/j.cma.2020.113493, 2021.

Feng, Y. T., Han, K., and Owen, D. R. J.: Energy-Conserving Contact Interaction Models for Arbitrarily Shaped Discrete Elements, Computer Methods in Applied Mechanics and Engineering, 205–208, 169–177, https://doi.org/10.1016/j.cma.2011.02.010, 2012.

Hopkins, M. A.: CN1 Numerical Simulation of Systems of Multitudinous Polygonal Blocks, CRREL report, 1992.

Hopkins, M. A.: On the Ridging of Intact Lead Ice, Journal of Geophysical Research: Oceans, 99, 16 351–16 360, https://doi.org/10.1029/94jc00996, 1994.

Hopkins, M. A.: Four Stages of Pressure Ridging, Journal of Geophysical Research: Oceans, 103, 21 883–21 891, https://doi.org/10.1029/98jc01257, 1998.

Hopkins, M. A., Hibler, W. D., and Flato, G. M.: On the Numerical Simulation of the Sea Ice Ridging Process, Journal of Geophysical Research: Oceans, 96, 4809–4820, https://doi.org/10.1029/90jc02375, 1991.

Hopkins, M. A., Tuhkuri, J., and Lensu, M.: Rafting and Ridging of Thin Ice Sheets, Journal of Geophysical Research: Oceans, 104, 13 605–13 613, https://doi.org/10.1029/1999jc900031, 1999.

Høyland, K. V.: Morphology and Small-Scale Strength of Ridges in the North-western Barents Sea, Cold Regions Science and Technology, 48, 169–187, https://doi.org/10.1016/j.coldregions.2007.01.006, 2007.

Itkin, P., Spreen, G., Hvidegaard, S. M., Skourup, H., Wilkinson, J., Gerland, S., and Granskog, M. A.: Contribution of Deformation to Sea Ice Mass Balance: A Case Study From an N-ICE2015 Storm, Geophysical Research Letters, 45, 789–796, https://doi.org/10.1002/2017gl076056, 2018.

Leppäranta, M. and Hakala, R.: The Structure and Strength of First-Year Ice Ridges in the Baltic Sea, Cold Regions Science and Technology, 20, 295–311, https://doi.org/10.1016/0165-232X(92)90036-T, 1992.

Lilja, V.-P., Polojärvi, A., Tuhkuri, J., and Paavilainen, J.: A Free, Square, Point-Loaded Ice Sheet: A Finite Element-Discrete Element Approach, Marine Structures, 68, 102 644, https://doi.org/10.1016/j.marstruc.2019.102644, 2019a.

https://doi.org/10.5194/egusphere-2024-831
Preprint. Discussion started: 13 May 2024
© Author(s) 2024. CC BY 4.0 License.

Lilja, V.-P., Polojärvi, A., Tuhkuri, J., and Paavilainen, J.: Effective Material Properties of a Finite Element-Discrete Element Model of an Ice Sheet, Computers & Structures, 224, 106 107, https://doi.org/10.1016/j.compstruc.2019.106107, 2019b.

Lilja, V.-P., Polojärvi, A., Tuhkuri, J., and Paavilainen, J.: Finite-Discrete Element Modelling of Sea Ice Sheet Fracture, International Journal of Solids and Structures, 217–218, 228–258, https://doi.org/10.1016/j.ijsolstr.2020.11.028, 2021.

Lipscomb, W. H., Hunke, E. C., Maslowski, W., and Jakacki, J.: Ridging, Strength, and Stability in High-resolution Sea Ice Models, Journal of Geophysical Research: Oceans (1978–2012), 112, https://doi.org/10.1029/2005jc003355, 2007.

Paavilainen, J., Tuhkuri, J., and Polojärvi, A.: 2D Combined Finite-discrete Element Method to Model Multi-fracture of Beam Structures, Engineering Computations, 26, 578–598, https://doi.org/10.1108/02644400910975397, 2009.

Parmerter, R. R. and Coon, M. D.: Model of Pressure Ridge Formation in Sea Ice, Journal of Geophysical Research, 77, 6565–6575, https://doi.org/10.1029/jc077i033p06565, 1972.

Polojärvi, A.: Numerical Model for a Failure Process of an Ice Sheet, Computers & Structures, 269, 106 828, https://doi.org/10.1016/j.compstruc.2022.106828, 2022.

Prasanna, M. and Polojärvi, A.: Breakage in Quasi-Static Discrete Element Simulations of Ice Rubble, International Journal of Mechanical Sciences, 259, 108 595, https://doi.org/10.1016/j.ijmecsci.2023.108595, 2023.

Ranta, J., Polojärvi, A., and Tuhkuri, J.: Limit Mechanisms for Ice Loads on Inclined Structures: Buckling, Cold Regions Science and Technology, 147, 34–44, https://doi.org/10.1016/j.coldregions.2017.12.009, 2018.

Roberts, A. F., Hunke, E. C., Kamal, S. M., Lipscomb, W. H., Horvat, C., and Maslowski, W.: A Variational Method for Sea Ice Ridging in Earth System Models, Journal of Advances in Modeling Earth Systems, 11, 771–805, https://doi.org/10.1029/2018ms001395, 2019.

Sanderson, T. J. O.: Ice Mechanics and Risks to Offshore Structures, 1988.

Schreyer, H. L., Sulsky, D. L., Munday, L. B., Coon, M. D., and Kwok, R.: Elastic-Decohesive Constitutive Model for Sea Ice, Journal of Geophysical Research: Oceans, 111, https://doi.org/10.1029/2005JC003334, 2006.

Schwarz, J.: New Developments in Modeling Ice Problem, in: Proc. of 4th POAC, vol. 1, pp. 45–61, 1977.

Sukhorukov, S. and Løset, S.: Friction of Sea Ice on Sea Ice, Cold Regions Science and Technology, 94, 1–12, https://doi.org/10.1016/j.coldregions.2013.06.005, 2013.

Thorndike, A. S., Rothrock, D. A., Maykut, G. A., and Colony, R.: The Thickness Distribution of Sea Ice, Journal of Geophysical Research, 80, 4501–4513, https://doi.org/10.1029/jc080i033p04501, 1975.

Timco, G. W.: Ice Forces on Structures: Physical Modelling Techniques, Second IAHR State-of-the-Art Report on Ice Forces on Structures, 4, 117–150, 1984.

Tuhkuri, J. and Lensu, M.: Laboratory Tests on Ridging and Rafting of Ice Sheets, Journal of Geophysical Research: Oceans (1978–2012), 107, 8–1–8–14, https://doi.org/10.1029/2001jc000848, 2002.

von Albedyll, L., Hendricks, S., Grodofzig, R., Krumpen, T., Arndt, S., Belter, H. J., Birnbaum, G., Cheng, B., Hoppmann, M., Hutchings, J., Itkin, P., Lei, R., Nicolaus, M., Ricker, R., Rohde, J., Suhrhoff, M., Timofeeva, A., Watkins, D., Webster, M., and Haas, C.: Thermodynamic and Dynamic Contributions to Seasonal Arctic Sea Ice Thickness Distributions from Airborne Observations, Elementa: Science of the Anthropocene, 10, https://doi.org/10.1525/elementa.2021.00074, 2022.